International Journal of Scholarly Research in
Biology and Pharmacy
Journal homepage: https://srrjournals.com/ijsrbp/
ISSN: 2961-3310 (Online)

(RESEARCH ARTICLE)

Computational identification of functionally important residues in Cytochrome P450 RufO

Harsh Khandagale † and Parinav Choudhury *, †

John Nash Fellowship, Mumbai, India.
† Contributed equally to this work.

International Journal of Scholarly Research in Biology and Pharmacy, 2026, 07(02), 044-050

Publication history: Received on 02 April 2026; revised on 13 May 2026; accepted on 15 May 2026

Article DOI: https://doi.org/10.56781/ijsrbp.2026.7.2.0026

Abstract

Aromatic nitration is an important chemical transformation widely used in the production of pharmaceuticals, dyes, agrochemicals, and energetic materials. However, conventional chemical nitration methods typically require harsh reaction conditions and often lack regioselectivity. In contrast, certain cytochrome P450 enzymes can catalyse selective aromatic nitration under mild biological conditions. RufO is a nitrating cytochrome P450 enzyme involved in the biosynthesis of the antibiotic rufomycin, where it catalyses nitration of a tyrosine residue within a precursor peptide. Despite its unique catalytic activity, the structural determinants governing substrate recognition and active-site organization in RufO remain poorly understood. In this study, we used computational structural analysis to identify residues that contribute to the functional architecture of RufO. We identified residues F69, T85, and M172 as important contributors to the local structural framework surrounding the catalytic pocket. Mutational analysis suggests that these residues primarily influence hydrogen-bonding networks, hydrophobic packing, and steric organisation rather than directly participating in catalysis. These findings also provide a foundation for future experimental studies aimed at understanding and engineering nitrating cytochrome P450 enzymes for selective nitroaromatic synthesis.

Keywords: Nitration; Cytochrome P450; Catalysis; Mutation; Enzyme engineering

1. Introduction

Nitroaromatics are aromatic compounds that have one or more nitro ($-NO_2$) groups attached directly to an aromatic ring. Some classic examples are nitrobenzene, dinitrobenzene, and 2,4,6-trinitrotoluene (TNT) [1]. There are also biologically derived molecules, such as 4-nitro-L-tryptophan [2] . Because the nitro group strongly pulls electrons away, these compounds have unique electronic properties. This makes them important for explosives, dyes, pigments, pharmaceuticals, agrochemicals, and as useful synthetic intermediates [1,3,4]. In industry, nitroaromatics are mainly produced through electrophilic aromatic substitution. This process uses concentrated nitric and sulfuric acids to produce the nitronium ion (NO_2^+). While this method is efficient for large-scale production, it often requires harsh conditions, has limited regioselectivity, and produces large amounts of corrosive acidic waste [5–7]. Moreover, many nitroaromatic compounds are toxic, persistent, and potentially mutagenic. These factors can lead to soil and groundwater contamination near manufacturing and military sites [8]. Such problems highlight the need for more selective and sustainable nitration methods.

Nature offers a more elegant solution through enzyme-catalysed aromatic nitration. So far, only two natural product biosynthetic enzymes can perform direct aromatic nitration: TxtE and RufO. TxtE is a bacterial cytochrome P450 found in *Streptomyces* species. It catalyses the regioselective conversion of L-tryptophan to 4-nitro-L-tryptophan using nitric oxide (NO), molecular oxygen (O_2), and reducing equivalents from NADPH [2,9]. A specific nitric oxide synthase

* Corresponding author: Parinav Choudhury

provides NO, forming an integrated NOS–P450 system that enables controlled nitration under mild conditions. Mechanistic studies show that TxtE stabilises a ferric-superoxo intermediate, which reacts with NO to form a peroxynitrite species [9,10]. This species is responsible for the selective C4 nitration of the indole ring. Structure-guided mutagenesis of active-site residues like Arg59, Asn293, Thr296, and Glu394 has shown that minor tweaks in substrate positioning and hydrogen-bonding networks can significantly change regioselectivity and catalytic efficiency [2,10]. This process emphasizes the precision needed for enzymatic nitration.

RufO is another cytochrome P450 involved in making rufomycin, a non-ribosomal peptide antibiotic [11]. Recent research suggests that RufO catalyses nitration within a ribosomally produced precursor peptide [12,13]. It adds a nitro group to a tyrosine residue, which is later incorporated into the mature rufomycin structure. This reaction illustrates how nature incorporates nitration into the assembly of complex secondary metabolites. However, in contrast to TxtE, the structural factors that influence substrate recognition, the catalytic mechanism, and regioselectivity in RufO are not well understood.

As the demand for greener nitration technologies grows, understanding and developing enzymatic nitrases is an appealing approach for sustainable nitroaromatic synthesis. While TxtE offers a clear framework for understanding the mechanics, RufO provides an opportunity to broaden the biocatalytic tools available for selective nitration. In this study, we use computational methods to identify critical residues in RufO, clarify the factors that influence substrate positioning and regioselectivity, and compare its active-site structure to that of TxtE. By revealing the molecular basis of RufO-mediated nitration, we aim to establish a groundwork for the informed engineering of nitrating P450s. This work could help in creating environmentally friendly methods for producing valuable nitroaromatic compounds.

2. Materials and Methods

2.1. Sequence Retrieval and Analysis

The amino acid sequences of TxtE (UniProt ID: C9ZDC6) and RufO (UniProt ID: A0A224AU14) were retrieved from the UniProt Knowledgebase (UniProtKB) [14]. The corresponding FASTA sequences were downloaded and served as reference sequences for residue numbering, domain annotation, and identifying conserved and active-site residues. This sequence information also guided structural mapping and mutational analysis.

2.2. Structural Data Collection

Experimentally determined three-dimensional structures were obtained from the Protein Data Bank (PDB) [15]. Structures were downloaded in .pdb format and used as reference models for structural comparison, active-site inspection, and alignment studies. When possible, crystal structures containing bound cofactors or substrates were prioritized to aid in understanding mechanisms.

2.3. Structure Modelling

Predicted wild-type protein structures were obtained from the AlphaFold [16]. For mutational analysis, site-directed amino acid substitutions were introduced directly into the primary sequence of the respective protein. The modified sequences were submitted to AlphaFold for structure prediction using default settings. The predicted mutant models were downloaded in .pdb format and compared structurally with their corresponding wild-type models. Comparisons focused on active-site structure, heme environment, substrate-binding pocket shape, and any changes in residue interactions.

2.4. Structural Visualization and Alignment

All structural visualization, superposition, residue mapping, and figure preparation were done using PyMOL (The PyMOL Molecular Graphics System, Schrödinger, LLC). Structural alignments used the built-in alignment algorithms in PyMOL to assess overall structural similarity and local shape differences, especially in the active site and substrate-binding regions. Images were prepared for publication-quality figures.

2.5. Protein–Ligand Interaction Analysis

Protein–ligand interactions were analysed using the Protein–Ligand Interaction Profiler (PLIP) web server with default settings [17]. The analysis identified hydrogen bonds, hydrophobic interactions, salt bridges, π–π stacking interactions, and metal coordination contacts. Interaction profiles were used to compare wild-type and mutant structures and evaluate changes in substrate positioning, catalytic geometry, and heme coordination.

2.6. Chemical Structure Preparation

Two-dimensional chemical structures and reaction schemes for TxtE- and RufO-related substrates and products were created using ACD/ChemSketch. These representations illustrated substrate structures, nitration sites, and proposed reaction mechanisms. The chemical diagrams were included in figures to support the mechanistic discussion in the manuscript.

3. Results

3.1. M172 Mutations

In the M172 structure (Figure 1A), the backbone of residue M172 participates in a hydrogen-bonding network with T382 and D169, helping stabilize the local conformation of the loop region. Substitution of methionine with phenylalanine M172F (Figure 1B) introduces a bulky aromatic ring that slightly alters the spatial arrangement of the surrounding residues, although the backbone hydrogen bonds with T382 and D169 remain largely preserved. When the same methionine is substituted with tyrosine M172Y (Figure 1C), it interacts with L168, contributing to hydrophobic packing and maintaining the structural integrity. In the M172W mutant (Figure 1D), the introduction of a larger tryptophan side chain further modifies the steric environment of the site, extending into the surrounding space while retaining the hydrogen-bonding interactions with T382 and D169. Here, although the core hydrogen-bonding network in this region is conserved, substitutions at position 172 modulate the local steric and hydrophobic environment, potentially influencing the structural dynamics and functional properties of the active site (Table 1).

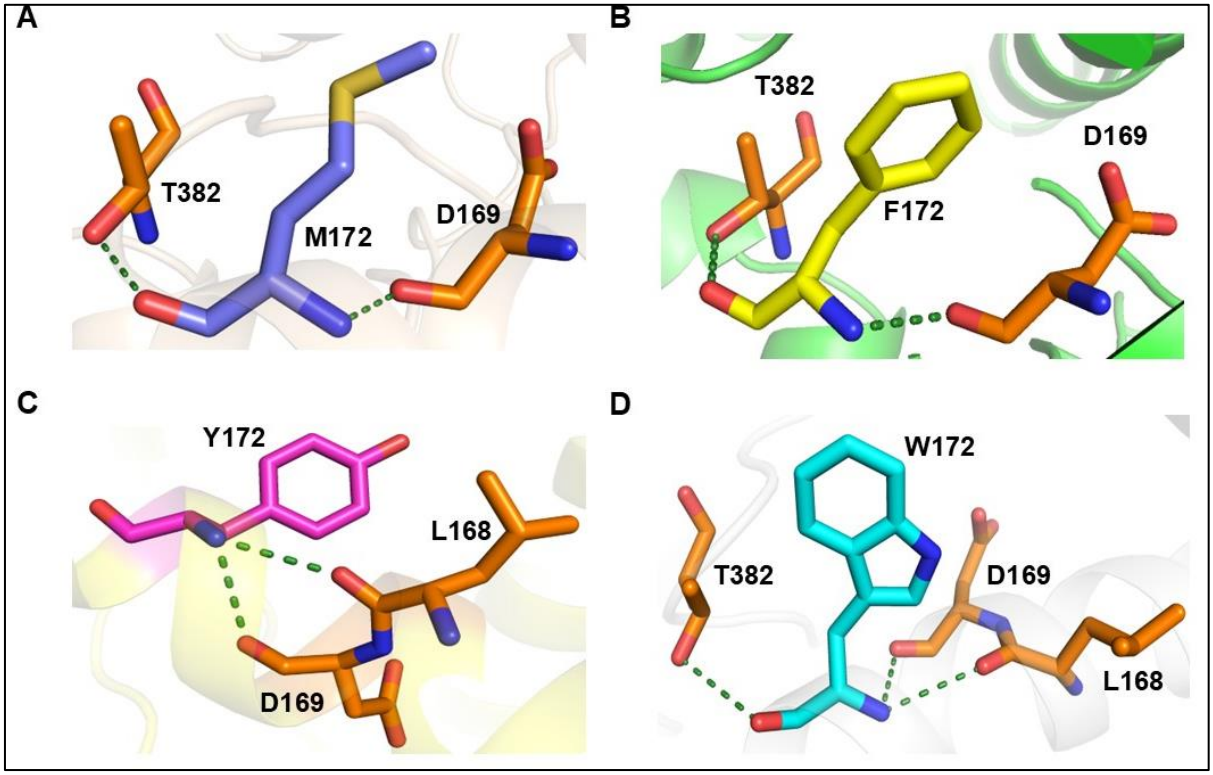

Figure 1 Comparison of interaction networks between wild type M172 and mutant M172F, M172Y and M172W

(A) Wild type M172 (blue sticks) interacts with T382 and D169 (orange sticks). (B) The mutant M172F (yellow sticks) forms similar interactions as that of the wild type. It interacts with T382 and D169 keeping the hydrogen bond network intact. (C) The mutant M172Y (magenta sticks) modifies the interactions. The interaction with T382 is disrupted but a new interaction with L168 establishes. (D) The mutant M172W (cyan sticks) includes the interactions of the wild type and the mutant. It keeps the wild type interactions intact and also introduces new interactions. It forms hydrogen bond with T382, D169 and L168. All the interactions are shown in green dashes.

3.2. T85 Mutations

Wild-type T85 establishes a hydrogen-bonding network with L80 and S82, supporting loop stability (Figure 2A). The T85F substitution disrupts the bond to L80, reducing polar interactions and leaving only partial contact with S82 (Figure 2B). This change shifts the region toward hydrophobic character without major backbone distortion (Table 1).

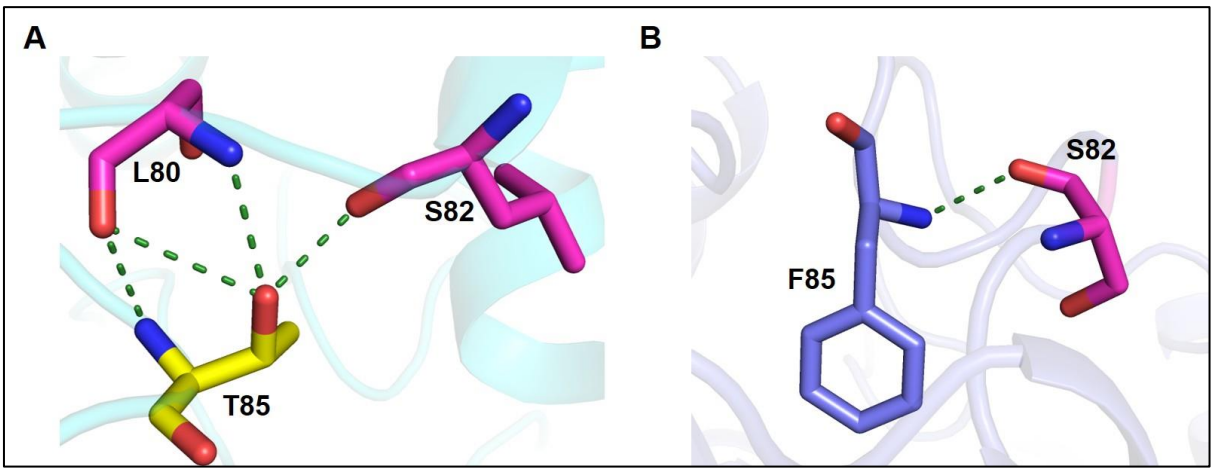

Figure 2 Comparison of interaction networks between wild type T85 and mutant T85F

(A) T85 (yellow sticks) forms hydrogen-bonding network L80 and S82 shown in magenta sticks. (B) The mutant T85F (blue sticks) the interaction with L80 is disrupted, leaving only a limited interaction with S82. All the interactions are shown in green dashes.

3.3. F69 Mutation

The F69 backbone in wild-type forms hydrogen bonds with T67, I72, and I74, aiding hydrophobic packing (Figure 3A). F69L mutation maintains these backbone interactions intact, preserving the hydrogen-bonding pattern despite reduced aromaticity (Figure 3B). Local packing remains stable with minimal perturbation (Table 1).

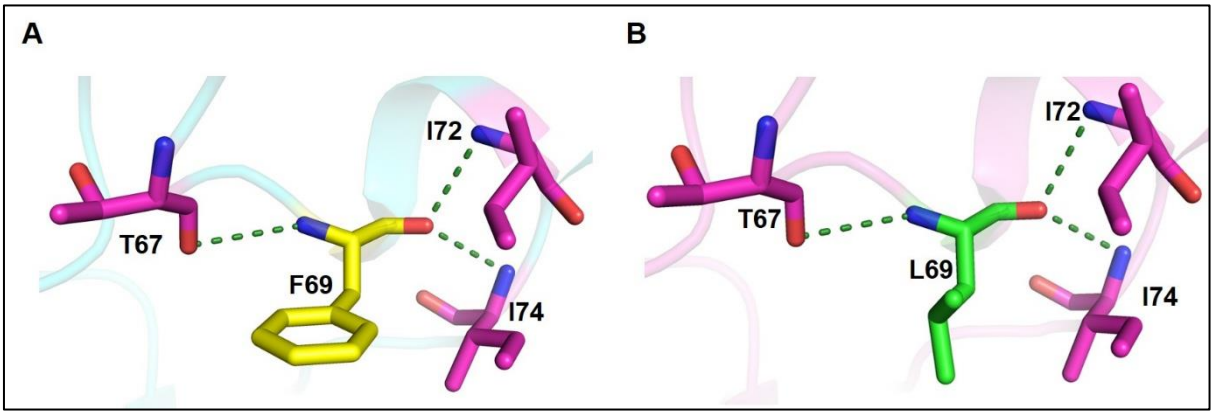

Figure 3 Comparison of interaction networks between wild type F69 (yellow sticks) to mutant F69L (green sticks)

(A) The backbone atoms of F69 form hydrogen-bonding interactions with T67, I72 and I74 represented as magenta sticks. (B) The mutant F69L does not distort the hydrogen bonding. The interactions with T67, I72 and I74 are intact. All the interactions are shown in green dashes.

3.4. T382 Mutation

Wild-type T382 interacts via hydrogen bonds with M172, D173, and Q284 (Figure 4A). The T382L mutant loses the M172 bond, resulting in a reorganized network limited to D173 and Q284 (Figure 4B). This alteration highlights T382's role in linking M172 to the broader structure (Table 1).

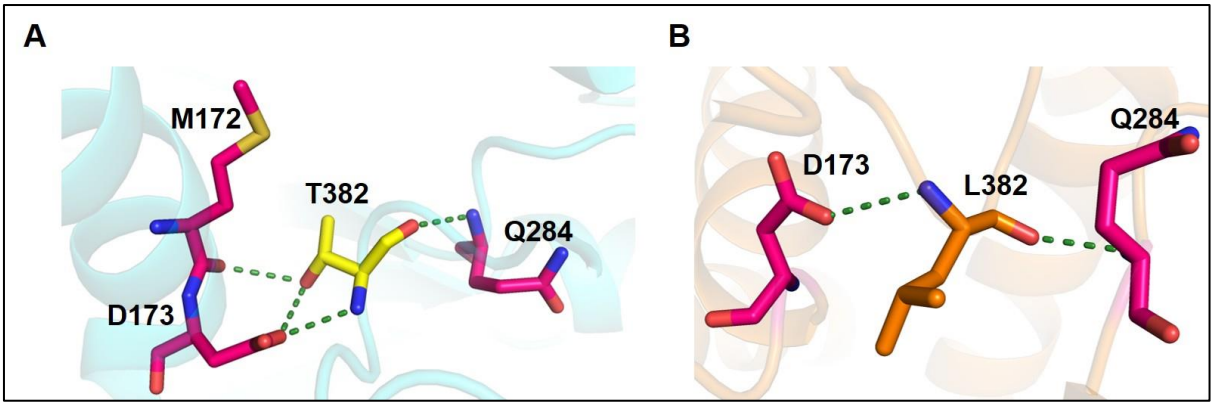

Figure 4 Comparison of interaction networks between wild type T382 (yellow sticks) and the mutant T382L (orange sticks)

(A) T382 interacts with M172, D173 and Q284. These are shown in magenta sticks. (B) Altered interaction pattern upon residue substitution T382L leading to a modified hydrogen-bonding network involving D173 and Q284. The interaction with M172 is lost. All the interactions are shown in green dashes.

Table 1 All the key interaction changes in RufO mutants across the four mutants

Residue	Wild Type Interactions	Mutant Changes
M172	H-bonds: T382, D169	Aromatic substitution add steric bulk; partial new contacts (L168 in M172Y/M172W)
T85	H-bonds: L80, S82	F85 disrupts L80 bond; polar loss
F69	Backbone H-bonds: T67, I72, I74	L69 preserves bonds; aromatic reduction
T382	H-bonds: M172, D173, Q284	L382 loses M172 bond

4. Discussion

Cytochrome P450 RufO is one of the few enzymes known to catalyse enzymatic aromatic nitration, yet the structural features that control its catalytic activity and substrate recognition remain poorly understood. In this study, computational structural analysis was used to identify residues that may contribute to the organization of the RufO active-site environment. The residues M172, T85, and F69 primarily influence the local structural architecture surrounding the catalytic pocket rather than directly participating in catalysis. Mutations at M172 indicate that while the backbone hydrogen-bonding network involving T382 and D169 remains conserved, substitutions with bulkier aromatic residues modify the steric environment of the region. Such changes may affect substrate positioning within the active site. Residue T85 appears to play a stabilizing role through its participation in a hydrogen-bonding network with L80 and S82. Mutating it with phenylalanine disrupts this polar interaction network and introduces a hydrophobic side chain, suggesting that T85 contributes to maintaining the structural integrity of the surrounding loop region. Another residue, F69, contributes to hydrophobic packing interactions that stabilise neighbouring residues T67, I72, and I74. Substitution with leucine reduces aromatic interactions while preserving the backbone hydrogen-bonding pattern, indicating that this position primarily influences local packing within the protein structure.

Overall, these observations suggest that residues surrounding the RufO catalytic pocket help maintain the structural framework that supports substrate binding and catalytic geometry. Similar structural roles have been observed in other cytochrome P450 enzymes, where residues outside the catalytic centre modulate substrate orientation and regioselectivity. The residues identified here therefore represent potential targets for future experimental mutagenesis studies aimed at understanding and engineering RufO-mediated nitration.

5. Conclusion

In this study, computational structural analysis was used to investigate residues that may contribute to the functional architecture of the cytochrome P450 nitrating enzyme RufO. Structural modelling and comparison of multiple residue variants revealed that residues F69, T85, and M172 play important roles in shaping the local structural environment surrounding the active site. While these residues do not directly coordinate the catalytic center, they influence hydrogen-bonding networks, hydrophobic packing, and steric constraints that stabilize the surrounding structural framework. The results suggest that RufO relies on a combination of structural stabilization and local packing interactions to maintain an active-site architecture suitable for selective aromatic nitration. Substitutions at key positions can alter the steric and polar environment of the catalytic pocket while preserving the overall structural scaffold of the enzyme. These findings provide insight into how local structural elements contribute to the functional organization of nitrating cytochrome P450 enzymes. Overall, this work establishes a structural basis for identifying functionally important residues in RufO and provides a foundation for future studies aimed at understanding its catalytic mechanism and engineering nitrating P450 enzymes for selective and sustainable synthesis of nitroaromatic compounds.

Compliance with ethical standards

Acknowledgments

The authors would like to thank Ms Saniya Dubey for mentoring and providing valuable suggestions for the studies. The authors would also like to thank the John Nash Thesis Fellowship for the resources and support provided for this research.

Disclosure of conflict of interest

No conflict of interest to be disclosed.

References

[1] K.-S. Ju, R.E. Parales, Nitroaromatic Compounds, from Synthesis to Biodegradation, Microbiol Mol Biol Rev 74 (2010) 250–272. https://doi.org/10.1128/MMBR.00006-10.

[2] S.C. Dodani, J.K.B. Cahn, T. Heinisch, S. Brinkmann-Chen, J.A. McIntosh, F.H. Arnold, Structural, functional, and spectroscopic characterization of the substrate scope of the novel nitrating cytochrome P450 TxtE, Chembiochem 15 (2014) 2259–2267. https://doi.org/10.1002/cbic.201402241.

[3] Explosives: Overview, (2023) 356–390. https://doi.org/10.1016/B978-0-12-823677-2.00143-4.

[4] Designing Drugs to Avoid Toxicity, in: Progress in Medicinal Chemistry, Elsevier, 2011: pp. 1–47. https://doi.org/10.1016/B978-0-12-381290-2.00001-X.

[5] N. Ran, L. Zhao, Z. Chen, J. Tao, Recent applications of biocatalysis in developing green chemistry for chemical synthesis at the industrial scale, Green Chem. 10 (2008) 361–372. https://doi.org/10.1039/B716045C.

[6] U.T. Bornscheuer, G.W. Huisman, R.J. Kazlauskas, S. Lutz, J.C. Moore, K. Robins, Engineering the third wave of biocatalysis, Nature 485 (2012) 185–194. https://doi.org/10.1038/nature11117.

[7] M.T. Reetz, Biocatalysis in organic chemistry and biotechnology: past, present, and future, J Am Chem Soc 135 (2013) 12480–12496. https://doi.org/10.1021/ja405051f.

[8] Nitroaromatic compounds: Environmental toxicity, carcinogenicity, mutagenicity, therapy and mechanism - Kovacic - 2014 - Journal of Applied Toxicology - Wiley Online Library, (n.d.). https://analyticalsciencejournals.onlinelibrary.wiley.com/doi/10.1002/jat.2980?utm_source=researchgate.net&utm_medium=article (accessed March 4, 2026).

[9] S. Louka, S.M. Barry, D.J. Heyes, M.Q.E. Mubarak, H.S. Ali, L.M. Alkhalaf, A.W. Munro, N.S. Scrutton, G.L. Challis, S.P. de Visser, Catalytic Mechanism of Aromatic Nitration by Cytochrome P450 TxtE: Involvement of a Ferric-Peroxynitrite Intermediate, J Am Chem Soc 142 (2020) 15764–15779. https://doi.org/10.1021/jacs.0c05070.

[10] R. Saroay, G.-D. Roiban, L.M. Alkhalaf, G.L. Challis, Expanding the Substrate Scope of Nitrating Cytochrome P450 TxtE by Active Site Engineering of a Reductase Fusion, ChemBioChem 22 (2021) 2262–2265. https://doi.org/10.1002/cbic.202100145.

[11] H. Tomita, Y. Katsuyama, H. Minami, Y. Ohnishi, Identification and characterization of a bacterial cytochrome P450 monooxygenase catalyzing the 3-nitration of tyrosine in rufomycin biosynthesis, J Biol Chem 292 (2017) 15859–15869. https://doi.org/10.1074/jbc.M117.791269.

[12] K. Nolan, R. Usai, B. Li, S. Jordan, Y. Wang, Molecular Basis for Peptide Nitration by a Novel Cytochrome P450 Enzyme in RiPP Biosynthesis, ACS Catal. (2025) 10391–10404. https://doi.org/10.1021/acscatal.5c01932.

[13] L. Padva, L. Zimmer, J. Gullick, Y. Zhao, V.M. Sasi, R.B. Schittenhelm, C.J. Jackson, M. Cryle, M. Crüsemann, Nitration of a ribosomal pentapeptide generates a noncanonical precursor for nonribosomal peptide synthesis, (2024). https://doi.org/10.1101/2024.07.12.603347.

[14] UniProt: the Universal Protein Knowledgebase in 2025 | Nucleic Acids Research | Oxford Academic, (n.d.). https://academic.oup.com/nar/article/53/D1/D609/7902999?login=true (accessed March 4, 2026).

[15] H.M. Berman, J. Westbrook, Z. Feng, G. Gilliland, T.N. Bhat, H. Weissig, I.N. Shindyalov, P.E. Bourne, The Protein Data Bank, Nucleic Acids Res 28 (2000) 235–242. https://doi.org/10.1093/nar/28.1.235.

[16] M. Varadi, D. Bertoni, P. Magana, U. Paramval, I. Pidruchna, M. Radhakrishnan, M. Tsenkov, S. Nair, M. Mirdita, J. Yeo, O. Kovalevskiy, K. Tunyasuvunakool, A. Laydon, A. Žídek, H. Tomlinson, D. Hariharan, J. Abrahamson, T. Green, J. Jumper, E. Birney, M. Steinegger, D. Hassabis, S. Velankar, AlphaFold Protein Structure Database in 2024: providing structure coverage for over 214 million protein sequences, Nucleic Acids Research 52 (2024) D368–D375. https://doi.org/10.1093/nar/gkad1011.

[17] M.F. Adasme, K.L. Linnemann, S.N. Bolz, F. Kaiser, S. Salentin, V.J. Haupt, M. Schroeder, PLIP 2021: expanding the scope of the protein–ligand interaction profiler to DNA and RNA, Nucleic Acids Research 49 (2021) W530–W534. https://doi.org/10.1093/nar/gkab294.